OXFORD

Reduced synaptic depression in human neurons carrying homozygous disease-causing *STXBP1* variant L446F

Miriam Öttl[1], Ruud F. Toonen[1], Matthijs Verhage [iD][1,2,*]

[1]Department of Functional Genomics, Center for Neurogenomics and Cognitive Research, Vrije Universiteit Amsterdam, De Boelelaan 1085, Amsterdam 1081HV, the Netherlands

[2]Department of Human Genetics, Center for Neurogenomics and Cognitive Research, University Medical Center, De Boelelaan 1117, Amsterdam 1081HV, the Netherlands

*Corresponding author. Department of Functional Genomics, Center for Neurogenomics and Cognitive Research, Vrije Universiteit Amsterdam, Amsterdam 1081HV, the Netherlands. E-mail: m.verhage@vu.nl

Abstract

MUNC18-1 is an essential protein of the regulated secretion machinery. *De novo*, heterozygous mutations in *STXBP1*, the human gene encoding this protein, lead to a severe neurodevelopmental disorder. Here, we describe the electrophysiological characteristics of a unique case of *STXBP1*-related disorder caused by a homozygous mutation (L446F). We engineered this mutation in induced pluripotent stem cells from a healthy donor ($STXBP1^{LF/LF}$) to establish isogenic cell models. We performed morphological and electrophysiological analyses on single neurons grown on glial micro-islands. Human $STXBP1^{LF/LF}$ neurons displayed normal morphology and normal basal synaptic transmission but increased paired-pulse ratios and charge released, and reduced synaptic depression compared to control neurons. Immunostainings revealed normal expression levels but impaired recognition by a mutation-specific MUNC18-1 antibody. The electrophysiological gain-of-function phenotype is in line with earlier overexpression studies in *Stxbp1* null mouse neurons, with some potentially human-specific features. Therefore, the present study highlights important differences between mouse and human neurons critical for the translatability of pre-clinical studies.

Keywords: STXBP1; epilepsy; electrophysiology; induced pluripotent stem cells; CRISPR

Introduction

Neurotransmission is the fundament on which the functioning of the brain is built. It depends on the coordinated assembly of SNARE (soluble N-ethylmaleimide-sensitive-factor attachment receptor) proteins which leads to the fusion of neurotransmitter-filled vesicles with the plasma membrane. The fusion process is strongly regulated [1]. One essential regulatory protein is Munc18-1. It chaperones the SNARE protein syntaxin-1 to form a complex with its partner SNAREs, thereby regulating all major steps in the fusion process: docking, priming, and fusion of vesicles [1, 2]. The absence of Munc18-1 in mouse neurons leads to a loss of neurotransmission and neuronal cell death [3, 4]. Heterozygous deletion primarily affects the size of the pool of vesicles that are ready to fuse upon arrival of an action potential, but does not lead to reduced evoked release [5]. In human neurons, on the other hand, heterozygous deletion of *STXBP1*, the human gene encoding MUNC18-1, has a profound impact on evoked and spontaneous release, while full deletion leads to cell death, albeit slower compared to mouse neurons [6, 7].

Recently, evidence is emerging that *de novo* heterozygous mutations in the genes encoding SNAREs and their regulatory proteins can lead to severe neurodevelopmental disorders, collectively termed "SNAREopathies" [8]. Indeed, mutations in *STXBP1* are associated with various cases of neurodevelopmental delay and encephalopathies, with most common symptoms

being epilepsy, motor problems and intellectual disability [9–11]. As *de novo* mutations, disease-causing variants of *STXBP1* are generally heterozygous and the disease mechanism is believed to be haploinsufficiency due to degradation of the mutated protein. However, we have previously reported an exceptional case of two siblings homozygous for the same *STXBP1* missense variant L446F [12]. Both siblings were diagnosed with Lennox-Gastaut syndrome, an epileptic encephalopathy [12, 13]. The mother and another sibling are heterozygous carriers of the same mutation and asymptomatic [12]. To understand the pathogenic mechanism, we expressed the mutant variant in *Stxbp1* null mouse neurons. Compared to null mutant neurons re-expressing wildtype Munc18-1 these neurons exhibited reduced neurite outgrowth and increased synaptic transmission including reduced paired-pulse ratios, implying increased release probability [12]. Intriguingly, this phenotype had not been observed when overexpressing a variety of other disease-associated mutant variants in mouse heterozygous or homozygous null mutant neurons [14]. Hence, the L446F mutation results in a unique cellular phenotype that translates in a shared clinical phenotype. However, it is not known whether these findings in mouse neurons can be translated directly to human neurons.

Human glutamatergic neurons can be generated by overexpression of the transcription factor neurogenin-2 (NGN2) in induced pluripotent stem cells (iPSCs) and the addition of small
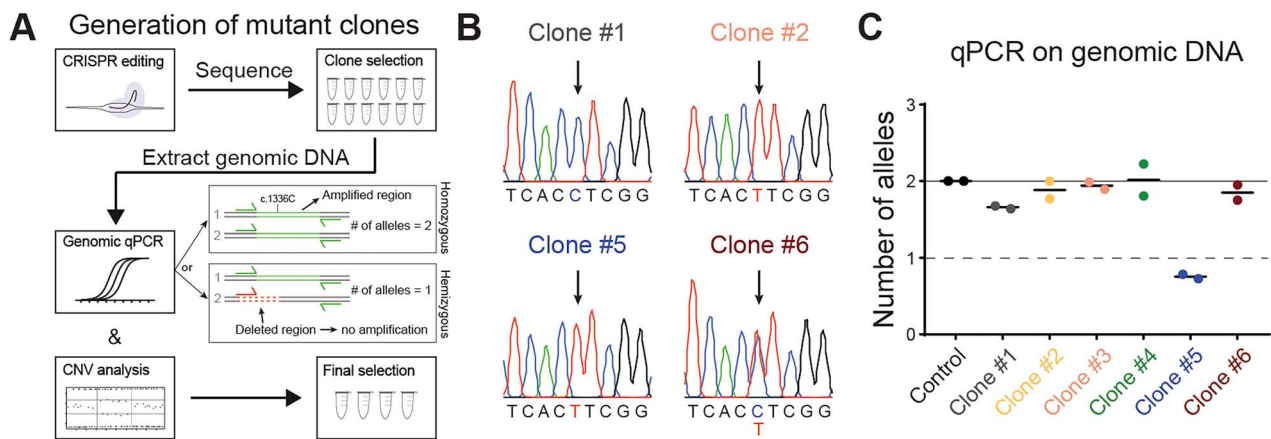
Figure 1. Selection and quality control of CRISPR/Cas9 edited iPSCs. (A) Selection workflow: After the CRISPR reaction and single-cell picking, clones were sequenced and selected based on successful edit. Then, high-quality DNA was extracted from the selected clones and qPCR on genomic DNA was performed as well as copy number variant (CNV) analysis, on which the final selection of clones was based. The inset shows the principle of genomic qPCR where, in a hemizygous clone, a loss of a gene fragment abolishes the binding of a primer, which leads to amplification of the intact gene only. This results in an allele number of 1 in the analysis, as opposed to a number of 2 when both alleles are intact. (B) Electropherograms from example clones showing the site of the mutation. The arrows point to position c.1336 which is mutated C > T, appearing homozygous in clones #2 and #5 and heterozygous in clone #6. (C) Number of alleles as calculated from qPCR on genomic DNA. Most clones show allele numbers of 2 except for #5 which is hemizygous due to an allele number of 1. Note that this clone appears homozygous from sequencing shown in B. Dots show data from 2 technical replicates. Lines show means of replicates.

molecules to steer them towards a cortical-like fate [15–20]. This technology greatly improves the translatability of studies aiming to understand human diseases. Here, we genetically modified iPSCs derived from a healthy donor using CRISPR/Cas9 to harbor the homozygous L446F *STXBP1* mutant variant (*STXBP1*$^{LF/LF}$), thereby creating isogenic lines that only vary in this specific mutation. Interestingly, human *STXBP1*$^{LF/LF}$ neurons showed a gain-of-function phenotype as observed in mouse neurons but with some important differences. Human *STXBP1*$^{LF/LF}$ neurons displayed normal morphology, normal spontaneous and evoked release, but increased paired-pulse ratios. In addition, high-frequency stimulation revealed that the neurons had slightly larger pools of releasable vesicles. Overall, this shows that *STXBP1*$^{LF/LF}$ neurons have altered synaptic plasticity in part via increased vesicle pools, leading to reduced synaptic depression.

Results
### Selection and quality control of CRISPR/Cas9 edited homozygous *STXBP1*$^{LF/LF}$ iPSCs

Forced expression of mouse *Stxbp1*$^{LF/LF}$ in primary mouse neurons devoid of endogenous Munc18-1 leads to a strong phenotype compared to overexpression of *Stxbp1*$^{WT/WT}$ [12]. In the present study, we generated human *STXBP1*$^{LF/LF}$ and isogenic control *STXBP1*$^{WT/WT}$ iPSC-derived neurons to increase translatability by generating a more disease-relevant model.

iPSCs from a healthy donor were engineered with CRISPR/Cas9 to harbor the *STXBP1* c.1336C>T (p.L446F) variant on both alleles, as evidenced by Sanger sequencing (Fig. 1A and B). In a recent study, it was shown that up to 40% of edited clones that appear homozygous in Sanger sequencing can in fact be hemizygous due to mono-allelic deletions of the gene or a gene fragment during editing, rendering them heterozygous knockouts instead [21]. To test for hemizygosity we performed quantitative PCR on genomic DNA (gqPCR) using primers 285 bp around the mutation, following the protocol by Weisheit *et al.* [22]. We analyzed 4 clones (clones #2-5) with an apparently homozygous knock-in of the mutation based on Sanger sequencing, one apparent heterozygote (clone

#6), and one apparent wildtype (WT) clone (clone #1), and compared them to an unedited clone of the same genetic background (Control; Fig. 1B and C). The control, WT and heterozygous clones had an allele number of 2, as had 3 out of the 4 homozygous clones (Fig. 1C). However, one of the homozygous clones (clone #5) had an allele number of 1, indicative of a mono-allelic deletion and, thus hemizygous (i.e. a false-positive homozygote) (Fig. 1C). This clone was rejected from further experiments. As additional quality control, we performed copy number variant (CNV) analysis to confirm that the edited clones did not acquire new large CNVs during the editing process. All clones passed this step. We selected the homozygous clones #2 and #3, the WT (clone #1) and the heterozygous clone (clone #6) for our experiments.

MUNC18-1 L446F is expressed normally but is not recognized by an antibody whose epitope spans the mutation site

Hippocampal glutamatergic mouse neurons overexpressing *Stxbp1*$^{LF/LF}$ have smaller dendritic trees and slightly reduced synapse numbers compared to controls [12]. To test if this phenotype is also present in human *STXBP1*$^{LF/LF}$ neurons, we generated human glutamatergic neurons via forced expression of NGN2 [18, 20] and performed immunostainings to measure dendrite length and synapse numbers. Single isolated neurons were cultured for 6 weeks on prepatterned glia microdot islands [17, 23]. In contrast to mouse neurons, both homozygous *STXBP1*$^{LF/LF}$ human clones as well as the heterozygous *STXBP1*$^{LF/WT}$ clone showed similar dendrite length and synapse density compared to the control clone *STXBP1*$^{WT/WT}$ (Fig. 2A–C). We then analyzed MUNC18-1 expression levels using two antibodies raised against different regions of MUNC18-1 (Fig. 3A). Antibody A detects the last 14 amino acids of the isoform of MUNC18-1 most expressed in glutamatergic neurons (Uniprot ID: P61764-1). Using this antibody, expression levels of MUNC18-1 in soma and synapses were identical between all genotypes (Fig. 3B–D). The epitope of antibody B covers the L446F mutation site. This antibody was unable to detect the mutated protein as in both homozygous clones the fluorescence intensity was close to
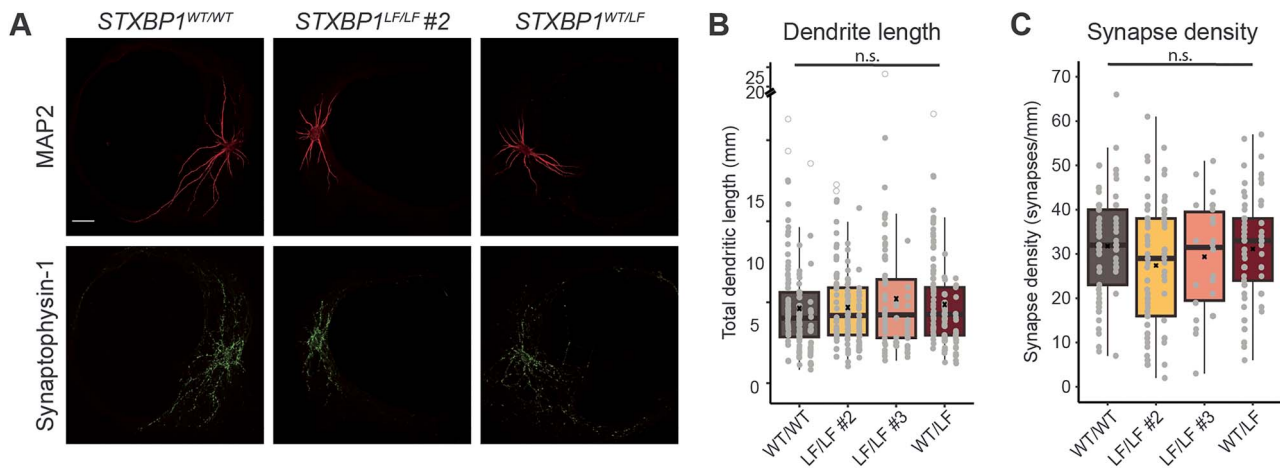
Figure 2. *STXBP1*^{LF/LF} neurons have normal morphology. (A) Example images of human single isolated glutamatergic neurons from *STXBP1*^{WT/WT}, the *STXBP1*^{LF/LF} clone #2 (as in Fig. 1) and the *STXBP1*^{WT/LF} clone. Neurons were stained for MAP2 and synaptophysin-1 to analyze dendritic length and synapse density, respectively. Scale bar = 50 μm. (B) Total dendrite length was based on a MAP2 mask for each cell. (C) Synapse density per mm dendrite was based on the number of synaptophysin-1-positive puncta within the MAP2 mask.

zero and the heterozygous clone showed a 50% reduction in fluorescence levels compared to control both in somas and synapses (Fig. 3E–G). We then performed Western blot analyses using the same two antibodies. We received similar results as from the cellular staining for both antibodies (Fig. 3H and I), showing that the mutated protein is normally expressed but that it is less detected by antibody B, albeit more than in knockout neurons. These results indicate that the L446F mutation does not affect MUNC18-1 expression or stability and that the mutated protein does not interfere with expression of MUNC18-1 from the WT allele. However, the L446F mutation changes the protein enough to interfere with binding of an antibody.

Basal synaptic transmission is unaffected in *STXBP1*^{LF/LF} neurons

Next, we performed patch-clamp electrophysiology on the homozygous *STXBP1*^{LF/LF} neurons and the *STXBP1*^{WT/WT} neurons at 6 weeks in culture (Fig. 4). Both *STXBP1*^{LF/LF} clones showed normal spontaneous vesicle release as miniature excitatory postsynaptic current (mEPSC) frequency and amplitude were similar compared to *STXBP1*^{WT/WT} (Fig. 4A–C). Furthermore, evoked EPSC amplitude and charge in *STXBP1*^{LF/LF} neurons were similar to *STXBP1*^{WT/WT} (Fig. 4D–F). Hence, in contrast to mouse *Stxbp1* null mutant neurons expressing Munc18-1 L446F [12], basal synaptic transmission in human *STXBP1*^{LF/LF} neurons is not altered.

Less synaptic depression in *STXBP1*^{LF/LF} neurons

The ratio between synaptic responses to two successive stimuli given at various time intervals (paired-pulse ratio; PPR) is typically used as a measure for release probability (Pr) [24–26]. We computed PPRs upon paired stimulations with 50, 100, 500 and 1000 ms intervals (Fig. 5A–C). The PPRs were increased in *STXBP1*^{LF/LF} neurons compared to *STXBP1*^{WT/WT} in most intervals (Fig. 5A–C). This suggests that *STXBP1*^{LF/LF} neurons have a lower release probability compared to controls. This result was unexpected as there was no difference in single evoked EPSC amplitudes (Fig. 4D–F), implying that the second pulse was driving the phenotype instead. Indeed, the absolute EPSC amplitude of the second pulse was larger compared to controls, while the first amplitude was similar (Fig. S1A and B). The phenotype can

therefore be best described as reduced synaptic depression and, thus, a gain-of-function.

Next, we stimulated the neurons with 100 pulses at 40 Hz to evoke the release of all readily releasable vesicles (Fig. 5D). As in the paired-pulse paradigm, *STXBP1*^{LF/LF} neurons displayed less depression compared to *STXBP1*^{WT/WT}, especially evident during the first few pulses (Fig. 5D–F). As the release pools in all groups were fully depleted and EPSCs converged to steady state by pulse 10, we analyzed the total charge released in the first 10 pulses to get an estimation of the number of vesicles available for release. The charge released in the first 10 pulses was significantly higher in *STXBP1*^{LF/LF} clone #2 compared to *STXBP1*^{WT/WT} (Fig. 5G), indicating that the cells had more releasable vesicles or enhanced vesicle recycling. Both possibilities may contribute to the reduced depression observed in *STXBP1*^{LF/LF} neurons.

Discussion

In this study, we generated isogenic iPSC lines carrying the disease-causing *STXBP1* missense mutation L446F in a healthy control genetic background (Fig. 1). We show that glutamatergic neurons derived from these iPSCs have normal morphology and basal synaptic transmission (Figs 2 and 4), but an increased paired pulse ratio, increased charge transferred, and reduced depression upon repeated stimulation (Fig. 5).

The L446F mutation is an exceptional case compared to most other disease-causing *STXBP1* mutations as only homozygous carriers experience disease symptoms and the mutation does not lead to lower cellular protein levels (Fig. 2; [12]), as is the case for other disease-causing mutations [9, 14, 27–30]. Thus, haploinsufficiency, the disease mechanism for most heterozygous *STXBP1* mutations currently studied, and confirmed in patient-derived neurons [27], cannot explain the phenotype seen here. Rather, the L446F mutation leads to an altered function of the MUNC18-1 protein. The mutation lies within domain 3b of the MUNC18-1 protein. Murine Munc18-1 depends on its domains 1 and 3a, which are essential for its functions and have been studied most extensively [1, 31–39]. In comparison, domain 3b is less explored and its role in Munc18-1's function is not fully understood yet. However, we have previously shown that phosphorylation of Y473, a residue at the edge of domain 3b, abolishes Munc18-1's priming but not docking abilities [40]. Domain 3b also binds the
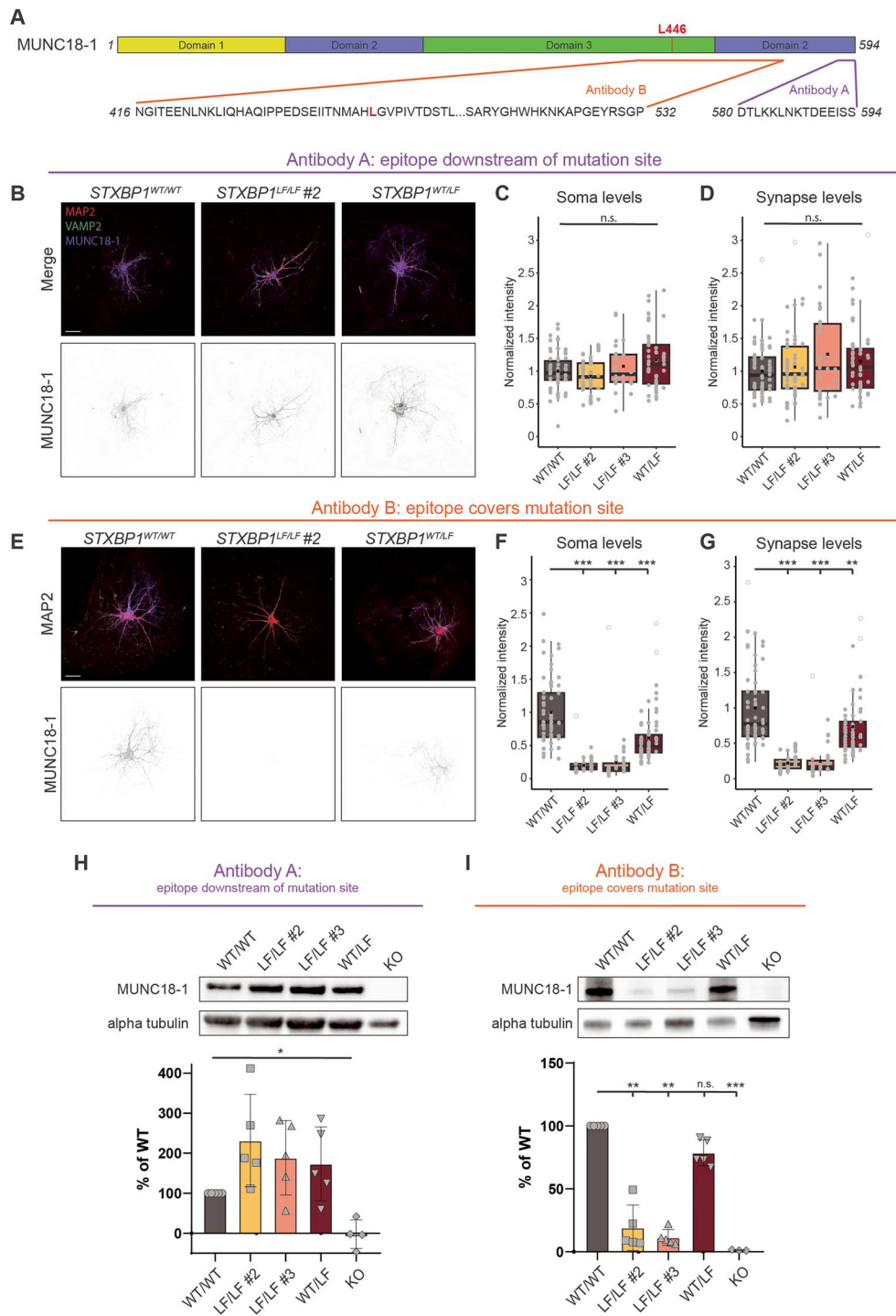
Figure 3. The L446F mutation leads to impaired recognizability by an antibody. (A) Scheme of the MUNC18-1 protein (Uniprot ID: P61764-1) showing its functional domains. The two antibodies used for detection of MUNC18-1 are indicated with the amino acid sequences they were raised against. Antibody A is specific for the last 14 amino acids of the isoform mostly expressed in NGN2 neurons. The L446 residue (marked by a line within domain 3) lies within the epitope of antibody B which recognizes all isoforms. (B) Example images of neurons from $STXBP1^{WT/WT}$, the $STXBP1^{LF/LF}$ clone #2 and the $STXBP1^{WT/LF}$ clone stained for MUNC18-1 using an antibody specific for the short isoform of MUNC18-1 (antibody A). Scale bar = 50 μm. (C) MUNC18-1 staining intensity using antibody A was measured within the soma (based on the MAP2 mask) and normalized to wildtype (WT) per experimental week. (D) MUNC18-1 staining intensity using antibody A was measured within synapses (based on the synaptophysin-1 mask) and normalized to wildtype (WT) per experimental week. (E) Example images of neurons stained for MUNC18-1 using an antibody with an epitope that covers the mutation site (antibody B). Scale bar = 50 μm. (F) MUNC18-1 staining intensity using antibody B was measured within the soma (based on the MAP2 mask) and normalized to wildtype (WT) per experimental week. (G) MUNC18-1 staining intensity using antibody B was measured within synapses (based on the synaptophysin-1 mask) and normalized to wildtype (WT). This antibody cannot detect MUNC18-1 with the L446F mutation. (H) Western blot performed using antibody A. MUNC18-1 bands were normalized to corresponding tubulin bands and then the percent of $STXBP1^{WT/WT}$ level was calculated per experimental week. (I) Western blot performed using antibody B. MUNC18-1 bands were normalized to corresponding tubulin bands and then the percent of $STXBP1^{WT/WT}$ level was calculated per experimental week. Boxplots show medians with interquartile range with whiskers extending to the most extreme data points within 1.5 times the interquartile range. One dot represents one cell, separated horizontally by experimental week. Outliers are shown as rings. Crosses show means. *$P < 0.05$, **$P < 0.005$, ***$P < 0.0005$.
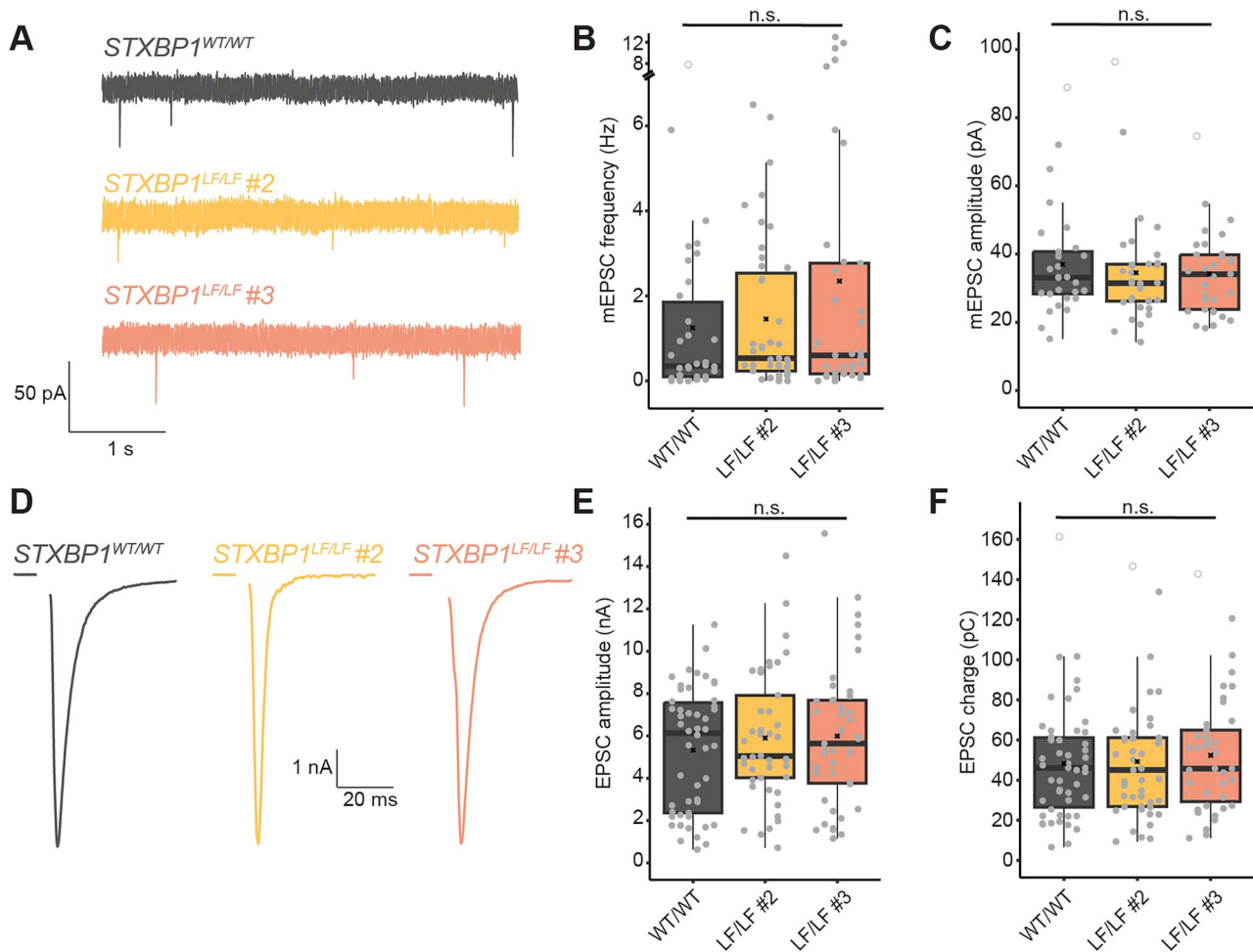
Figure 4. $STXBP1^{LF/LF}$ neurons display normal basal synaptic transmission. (A) Example traces of gap-free recordings showing mEPSCs of the control ($STXBP1^{WT/WT}$) and mutated clones ($STXBP1^{LF/LF}$ #2 and #3). (B) mEPSC frequency within 30 s recordings is not different between $STXBP1^{LF/LF}$ clones and $STXBP1^{WT/WT}$. (C) mEPSC amplitudes are not different between $STXBP1^{LF/LF}$ clones and $STXBP1^{WT/WT}$. (D) Example traces of single evoked EPSCs. (E) EPSC amplitudes of single stimulations of 1 ms (+30 mV) are not different between $STXBP1^{LF/LF}$ clones and $STXBP1^{WT/WT}$. (F) EPSC charge of single stimulations of 1 ms (+30 mV) is not different between $STXBP1^{LF/LF}$ clones and $STXBP1^{WT/WT}$. Boxplots show medians with interquartile range with whiskers extending to the most extreme data points within 1.5 times the interquartile range. One dot represents one cell, separated horizontally by experimental week. Outliers are shown as rings. Crosses show means.

Munc18-interacting proteins Mint-1/2 (also known as X11α/β) [41–43]. No direct involvement of residue L446 was reported for this interaction. However, the residue lies in close proximity to the residues that bind Mints [42] as well as other disease-related residues [12], and it resides close to a proposed Rab3a-binding region [44]. We show here using immunostainings on single cells that the L446F mutation disrupts the binding of a MUNC18-1-specific antibody whose epitope spans the mutation site (Fig. 3). This may suggest that the conformation of the protein is altered. However, we also find reduced binding of the same antibody with Western blotting, suggesting that the antibody recognition depends on the sequence rather than the structure of the protein. It is tempting to speculate that the Leucine to Phenylalanine change might instead result in altered interactions of MUNC18-1 with Mints or other binding partners, or possibly even recruit new binding partners, ultimately changing the function of the protein.

The phenotype of human $STXBP1^{LF/LF}$ neurons, as in mouse neurons, can be described as a gain-of-function [12]. However, the exact nature of the phenotype in human neurons is different compared to mouse, suggesting the possibility of a unique human signature. One explanation for this divergence could be the fact that in mouse neurons the mutant variant is delivered by virally induced overexpression compared to endogenous expression in the human neurons. It is possible that the exact expression levels of the mutant lead to different effects on the mechanisms of vesicle fusion. Indeed, expression levels of Munc18-1 have substantial effect on the size of the releasable vesicle pool and depression kinetics [5]. Another explanation could be that the mouse and human neurons were in different maturational stages at the time of the experiments. For example, the effect on morphological parameters of motor neurons by a mutation related to amyotrophic lateral sclerosis was found to be different throughout development of the cells [45]. In the present study, human neurons were recorded after 6 weeks in culture while the experiments in mouse neurons were performed 2 weeks after dissection. Neuronal development of human neurons derived from iPSCs takes multiple weeks with synapse development continuing throughout [17, 46]. In fact, 6 weeks old human neurons, despite showing electrophysiological activity, may only be as mature as mouse neurons in early postnatal development as reported for slices [18, 47]. Finally, differences in cellular phenotypes between mouse and human neurons may result from intrinsic species differences.
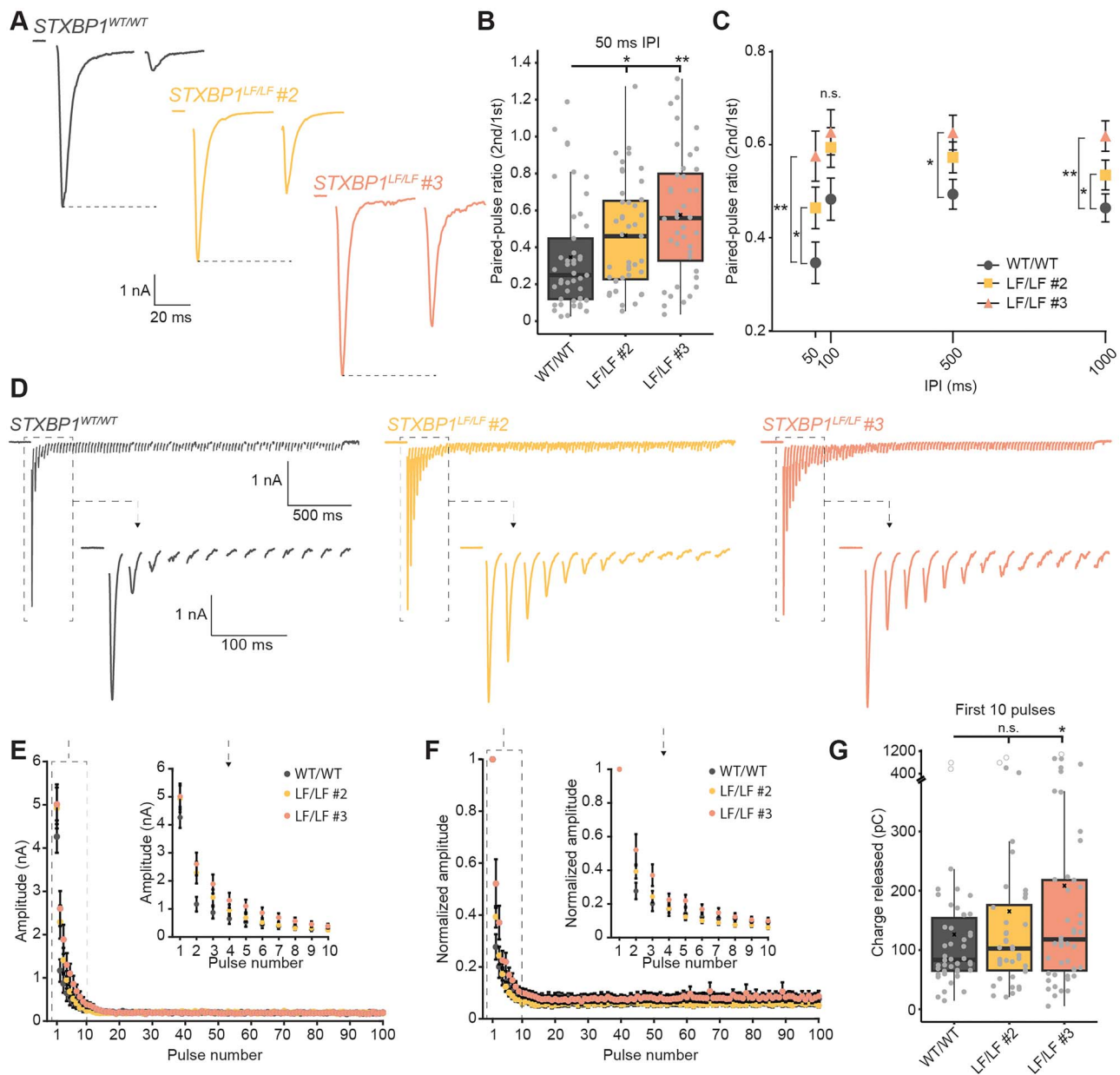
Figure 5. Less synaptic depression in *STXBP1*^LF/LF neurons. (A) Example traces of paired stimulations with 50 ms inter-pulse intervals. Dotted lines level at the peaks of each first amplitude. (B) The paired-pulse ratio (PPR) with 50 ms interval was calculated by dividing the second amplitude by the first. Both *STXBP1*^LF/LF clones show significantly higher PPRs compared to *STXBP1*^WT/WT. (C) Summary of paired-pulse ratios with different inter-pulse intervals (IPIs). (D) Example traces of recordings with 100 stimulations (1 ms to +30 mV) at 40 Hz. The first 10 pulses were additionally magnified (magnified part marked by a dashed box). (E) Absolute EPSC amplitudes from recordings exemplified in D were plotted by pulse number to visualize the rundown of release over time. The inset shows the same plot only for the first 10 pulses as marked by the dashed box. (F) Normalized EPSC amplitudes from recordings exemplified in D were plotted by pulse number to visualize the rundown of release over time. The inset shows the same plot only for the first 10 pulses as marked by the dashed box. (G) Total amount of charge released within the first 10 pulses of the 40 Hz stimulation as exemplified in D. In B and G, boxplots show medians with interquartile range with whiskers extending to the most extreme data points within 1.5 times the interquartile range. One dot represents one cell, separated horizontally by experimental week. Outliers are shown as rings. Crosses show means. In C, E and F, data are presented as means ± SEM. *P < 0.025, **P < 0.005.

Such a difference has recently been shown in a study comparing mouse and human microglia [48]. Most studies on the functions of the release machinery and Munc18-1 have been conducted using rodent neurons. It remains to be seen whether all mechanics of the rodent fusion machinery are identical in human neurons.

We engineered the L446F mutation in a healthy control iPSC line using CRISPR/Cas gene editing. In this design, the L446F mutation is the main genetic difference between the experimental and control group. Compared to classical rescue experiments in null mutant mouse neurons it offers the advantage of endogenous expression levels. This allows for direct assessment of the contribution of the mutation to the disease mechanism and offers higher statistical power compared to case–control designs in which patient-derived lines are compared to unrelated controls [49]. However, it does not test for potential interactions of the mutation with a patient's genetic background. Indeed, an interaction with a patient's specific genetic background was recently found for autism-related gene mutations [50], and genetic differences between healthy individuals have been shown to affect expression levels and morphology by large proportions [51–53].

Table 1. Guide RNA and ssODN sequences.

Variant	gRNA	ssODN
L446F	5′CACGCCGAGGTGAG CCATGT 3′	5′CCCCCGGAAGCTGAGCTGGCCTCTTACATCGGTGACGATGG GCACGCCGAAGTGAGCCATGTTTGTGATGATCTCACTATCCTC CGGGGGTATCTGGGCG 3′

Thus, it is conceivable that a neuronal phenotype may present differently depending on the genetic background of a cell line/individual. To test this, cells from patients should be compared to repaired patient-own isogenic cells.

In conclusion, our data show that the *STXBP1* L446F mutation in human neurons leads to a gain-of-function phenotype in synaptic transmission manifested as less depression during repetitive stimulation. These effects are caused by a change in functionality of the MUNC18-1 protein.

Materials and methods
CRISPR/Cas9 genome editing

The *STXBP1* variant L446F (NM_001032221.6:c.1336C>T; OMIM reference number 602926.0009) was engineered in the healthy control induced pluripotent stem cell (iPSC) line BIONi010-C-13 (EBiSC) using CRISPR/Cas9 technology. The sequences of the guide RNA (gRNA, Synthego) and single-stranded oligodeoxynucleotides (ssODN) repair template (Ultramer DNA Oligonucleotide, Integrated DNA Technologies) can be found in Table 1. Both constructs, as well as Cas9, were delivered into the iPSCs by nucleofection using a 4D-Nucleofector X Unit and using the Amaxa P3 primary cell 4D-nucleofector X kit S (V4XP-3032, Lonza). After nucleofection, the cells were cultured at 32°C for two days to promote editing. The edited cells were Sanger sequenced (Eurofins) and the editing efficiency was evaluated using TIDE [54]. When editing was confirmed, the cells were plated as single cells to obtain single clones as confirmed by sequencing. To confirm that the heterozygous clone is pure instead of a mixture of wildtype and edited cells, we plated single cells and confirmed the genotype in all derived clones again by sequencing. To test whether the cells acquired large deletions or insertions during the editing process we screened all clones for copy number variations (CNVs) via the Global Screening Array (GSA) Consortium Project at Erasmus MC (Rotterdam, the Netherlands) using Illumina GSA beadchip GSAMD-version 3 (Chromosome build 37). Arrays were processed in Genome studio 2.0. Illumina Genome Studio software was used to process and annotate SNP data and the iPsychCNV package for R was used to call CNVs [55]. DNA was extracted from dense iPSC cultures using the ReliaPrep gDNA Tissue MiniPrep System (Promega). Clones were only considered for use in experiments when their CNV calls overlapped with those of the wildtype clone.

qPCR on genomic DNA

Because of the possibility that CRISPR clones appearing as homozygous in sequencing could in fact lack one of their alleles (i.e. be hemizygous) [21], we performed quantitative PCR (qPCR) on the same genomic DNA as was used for CNV analysis (see above), following the protocol by Weisheit *et al.* [22] (Fig. 1). The primers used for qPCR can be found in Table 2. GAPDH, Myc and EIF4G2 were used as reference household genes, the geomean of all 3 was used for normalization of Ct values. Primers for *STXBP1* were designed according to Weisheit *et al.* [22] to receive a product covering the Cas9 cut site. NanoDrop was used to determine the DNA concentration, based on which solutions of 10 ng/μl were

made. The qPCR was performed using QuantStudio™ 5 Real-Time PCR System using SensiFAST SYBR Lox-ROX (Bioline), the program can be found in Table 3. Analysis was performed according to [22]. Only clones with an allele number of close to 2 were considered for experiments. One hemizygous clone was found and discarded (Fig. 1).

Cell culture and neuronal differentiation

iPSCs were maintained on Matrigel-coated plates (VWR) in Essential 8 (E8) medium supplemented with 0.1% Penicillin/Streptomycin (P/S, Fisher Scientific). BIONi010-C-13 iPSCs contain doxycycline-inducible neurogenin-2 (NGN2) within the AAVS1 safe-harbor locus [56]. Therefore, it was not necessary to infect the cells with a construct of the NGN2 gene for neuronal induction. Neuronal differentiation was started by transferring the iPSCs to Cultrex-coated dishes (3400-010-02, Bio-Techne) with DMEM/F12 (10565018, Gibco) supplemented with N2 supplement (Stemcell Technologies), 0.1% P/S, 200 mM GlutaMax (Life Tech; 11574466), 1.5% D-Glucose (20%, A2494001, Gibco), doxycycline hyclat (dox; 2 μg/ml, Sigma Aldrich), 5 μM ROCK-inhibitor (RI; Y-27632, Tebubio), as well as the SMAD inhibitors LDN-193189 (100 nM; Stemgent) and SB431542 (10 μM; Tocris), and the WNT inhibitor XAV939 (2 μM; Stemgent). On the following day, the cells were refreshed with the same medium but without ROCK-inhibitor. On the third day, the cells were refreshed with the same medium plus 10 μM FUDR (Sigma Aldrich). One day later, the neurons were plated on glia coverslips in neurobasal medium (NBM; 11570556, Gibco) supplemented with 200 mM Glutamax, D-Glucose, non-essential amino acids (NEAA; 11350912, Gibco), B27 (17504044, Gibco), 0.1% P/S, 0.5% Fetal bovine serum, dox, and growth factors BDNF, CNTF and GDNF (all 10 ng/ml, Stemcell Technologies). For electrophysiology and immunostainings, the cells were plated at a density of 2 k cells per 18 mm coverslip. Coverslips contained islands of glia as shown previously [17]. Briefly, glass coverslips were coated with agarose (Type II-A; Sigma, A9918) and stamped with a mixture of 0.1 mg/ml poly-D-lysine (Sigma, P6407), 0.7 mg/ml rat tail collagen (BD Biosciences, 354236), and 10 mM acetic acid (Sigma, 45731) using a custom-made stamp. Rat glia were plated at a density of 8 k per coverslip. Single neurons will attach to the glia islands and form synapses with themselves, called "autapses" [23]. Neurons were maintained at 37°C and 5% CO_2. Half of NBM was refreshed once a week. Experiments were performed on days 42 to 46 (6 weeks) after differentiation was started.

Electrophysiology

Whole-cell patch clamp electrophysiology in voltage-clamp configuration was performed after 6 weeks in culture. The autaptic neurons were placed in artificial cerebrospinal fluid (aCSF) containing (in mM): 10 HEPES, 10 Glucose, 140 NaCl, 2.4 KCl, 4 $MgCl_2$ and 4 $CaCl_2$ (pH = 7.30, ∼300 mOsmol). Borosilicate glass pipettes (Science products GmbH) were used at resistances of 2.5-4.5 MΩ and contained: 125 mM K^+-gluconic acid, 10 mM NaCl, 4.6 mM $MgCl_2$, 15 mM creatine phosphate, 10 U/ml

Table 2. Primers for qPCR on genomic DNA.

Gene (primer name)	Forward	Reverse
STXBP1	5′GCAATGTCCACTAACCCTGA 3′	5′CTCTTGACGTACGAGTGTGTATC 3′
GAPDH	5′GTTCGACAGTCAGCCGCATC 3′	5′TCCGTTGACTCCGACCTTCA 3′
Myc	5′CCCTCCACTCGGAAGGACTA 3′	5′GCTGGTGCATTTTCGGTTGT 3′
EIF4G2	5′AGGACCGCATGTTGGAGATT 3′	5′TGAGGGGATGGATCCAACTTT 3′

Table 3. qPCR program.

Stage	Temp	Time	Speed	Cycles
Hold stage	95 C	5 min	1.6 C/s	1
PCR stage 1	95 C	10 sec	1.6 C/s	40
PCR stage 2	60 C	20 sec	1.6 C/s	40
PCR stage 3	72 C	1 sec	1.6 C/s	40
Melt curve 1	95 C	15 sec	1.6 C/s	1
Melt curve 2	60 C	1 min	1.6 C/s	1
Melt curve 3	95 C	15 sec	0.075 C/s	1

phosphocreatine kinase, and 1 mM EGTA (pH 7.3, ~300 mOsmol). The recordings were made using an Axopatch 200B amplifier and Digidata 1440A digitizer, controlled by Clampex 10.6 software (Molecular Devices). Miniature excitatory postsynaptic currents (mEPSCs) were recorded at 20 kHz sampling rate and 5 kHz filtering rate using a low-pass Bessel filter. Stimulation protocols were sampled at 10 kHz with 2 kHz filtering. Compensation was set to 70% (bandwidth 7.52 Hz). Neurons were stimulated by setting the voltage to 30 mV for 1 ms. Recordings with series resistance of higher than 15 MΩ and leak current of more than 300 pA were excluded. Asynchronicity of single EPSCs was assessed by running the traces through an analysis pipeline described previously [49]. Recordings were deemed too asynchronous if the contribution of small additional peaks to the major peak was above the cutoff with user decision. Analysis of all recordings was performed in Matlab R2019a (Mathworks) using a custom-written software (viewEPSC, downloaded from user vhuson on Github). The experimenter was blinded during the experiment and analysis.

Immunocytochemistry

Neurons were fixed in 3.7% paraformaldehyde (PFA; Electron Microscopy Sciences) after 6 weeks in culture and immunostained to assess dendrite morphology, synapses, and MUNC18-1 expression. After fixation and three washes with phosphate buffered saline (PBS; pH ~7.4), the neurons were permeabilized by application of 0.5% triton X-100 (#T/3751/08, Thermo Fisher) for 5 min and incubated in blocking buffer (BB) for 30 min. BB contained 2% normal goat serum (#11540526, Thermo Fisher) and 0.1% triton X-100 in PBS. Next, neurons were incubated with primary antibodies diluted in BB for 2 h at room temperature. The following primary antibodies were used: chicken anti-MAP2 (1:500, Abcam Ab5392), guinea pig anti-synaptophysin-1 (1:1000, Synaptic Systems #101004) or mouse anti-VAMP2 (1:1000, Synaptic Systems #104211), and rabbit anti-Munc18-1b (antibody A; 1:1000, Synaptic Systems #116002) or rabbit anti-MUNC18-1 (antibody B; 1:250, Sigma, HPA023483). The neurons were then washed three times and incubated in secondary antibodies (Alexa Fluor, 1:1000) diluted in BB for 1 h at room temperature. After another three washes, coverslips were mounted on glass slides in Mowiol-DABCO. Images were acquired on a NIKON Ti-Eclipse microscope,

equipped with a confocal scanner model A1R+, using a 40X oil immersion objective (NA = 1.3, Carl Zeiss). For each cell, 5 planes were acquired in a z-stack with increments of 1.5 μm. Z-stacks were collapsed to maximal projections for image analysis using ImageJ. The images were analyzed using the semi-automated pipeline SynJ provided by Github user alemoro.

Western blot

High density neuronal cultures were lysed after 6 weeks in culture in Laemmli sample buffer and stored at −20 degrees. For Western blotting, lysates were boiled for 5 min and loaded on pre-cast sodium dodecyl sulfate (SDS) polyacrylamide gels with a 4%–20% gradient (#4568096, Bio-Rad). Proteins were resolved at 110 V and transferred to nitrocellulose membranes using semi dry Trans-Blot Turbo Transfer System (#1704150, Bio-Rad). Successful transfer was validated by Ponceau S staining of membranes. Membranes were blocked for 1 h in PBS containing 0.05% Tween-20 detergent (PBS-Tween) and 2% BSA. Thereafter, membranes were incubated overnight at 4°C with primary antibodies dissolved in blocking buffer. The following primary antibodies were used: polyclonal rabbit anti-Munc18-1b (antibody A; 1:1000, Synaptic Systems, 116002), or polyclonal rabbit anti-MUNC18-1 (antibody B; 1:1000, Sigma, HPA023483), mouse anti-alpha-tubulin (1:10000, Synaptic Systems, 302 211), and mouse anti-beta-3 tubulin (1:1000, Invitrogen, MA1-19187). Each membrane was incubated with one anti-Munc18-1 antibody and one anti-tubulin antibody at the same time. After the incubation with primary antibody solutions, membranes were washed three times in PBS-Tween and incubated for 1 h at room temperature with secondary antibodies IRDye 680LT goat anti-mouse (1:5000; LI-COR, 926-68 020) and IRDye 800CW goat anti-rabbit (1:5000; LI-COR, 926-32 211). Membranes were again rinsed three times in PBS-Tween and developed on the Odissey Fc imaging system (LI-COR Bioscience) using 2 min exposure time. Fluorescence signals were analyzed using Image Studio Lite Software. MUNC18-1 bands were normalized to corresponding tubulin bands and then the expression level in percent of control was calculated.

Statistical analysis

Statistical analysis on staining and electrophysiological data was performed using R (version 4.2.2). Due to the nested nature of

the data used here, we performed fixed linear regression analysis using the lm() function. First, outliers were removed when they were more than 3 times the standard deviation above or below the group mean. Then, the data were standardized to z-scores using grand mean centering before fitting them to the linear regression model. Two models were fitted, one without including group as predictor, and one including group as predictor. The experimental batch was always included as covariate. Statistical significance of adding group as predictor was determined by comparing the two models using one-way ANOVA (analysis of variance). When the significance level of 0.05 was met, post-hoc analysis was performed. For that, data were subset pairwise and linear regression fitting was repeated. P-value thresholds were Bonferroni-corrected to account for multiple testing. For Western blots, data were analyzed in GraphPad Prism (v.8.0.1) using Kruskal-Wallis test with Dunn's post-hoc comparisons.

Author contributions

All authors conceptualized the study together. M.Ö. performed all experiments and analyzed the data.

Supplementary data

Supplementary data is available at *HMG Journal* online.

Conflict of interest statement: The authors declare no competing interests.

Funding

References

1. Rizo J. Molecular mechanisms underlying neurotransmitter release. *Annu Rev Biophys* 2022;**51**:377–408.

2. Toonen RFG, Verhage M. Munc18-1 in secretion: lonely Munc joins SNARE team and takes control. *Trends Neurosci* 2007;**30**: 564–72.

3. Dudok JJ, Groffen AJA, Toonen RFT. *et al.* Deletion of Munc18-1 in 5-HT neurons results in rapid degeneration of the 5-HT system and early postnatal lethality. *PLoS One* 2011;**6**: e28137.

4. Verhage M, Maia AS, Plomp JJ. *et al.* Synaptic assembly of the brain in the absence of neurotransmitter secretion. *Science* 2000;**287**:864–9.

5. Toonen RFG, Wierda K, Sons MS. *et al.* Munc18-1 expression levels control synapse recovery by regulating readily releasable pool size. *Proc Natl Acad Sci USA* 2006;**103**:18332–7.

6. Patzke C, Han Y, Covy J. *et al.* Analysis of conditional heterozygous STXBP1 mutations in human neurons. *J Clin Invest* 2015; **125**:3560–71.

7. Santos TC, Wierda K, Broeke JH. *et al.* Early Golgi abnormalities and neurodegeneration upon loss of presynaptic proteins Munc18-1, Syntaxin-1, or SNAP-25. *J Neurosci* 2017;**37**: 4525–39.

8. Verhage M, Sørensen JB. SNAREopathies: diversity in mechanisms and symptoms. *Neuron* 2020;**107**:22–37.

9. Saitsu H, Kato M, Mizuguchi T. *et al.* De novo mutations in the gene encoding STXBP1 (MUNC18-1) cause early infantile epileptic encephalopathy. *Nat Genet* 2008;**40**:782–8.

10. Stamberger H, Nikanorova M, Willemsen MH. *et al.* STXBP1 encephalopathy: a neurodevelopmental disorder including epilepsy. *Neurology* 2016;**86**:954–62.

11. Xian J, Parthasarathy S, Ruggiero SM. *et al.* Assessing the landscape of STXBP1-related disorders in 534 individuals. *Brain* 2022;**145**:1668–83.

12. Lammertse HCA, van Berkel AA, Iacomino M. *et al.* Homozygous STXBP1 variant causes encephalopathy and gain-of-function in synaptic transmission. *Brain* 2020;**143**:441–51.

13. Cross JH, Auvin S, Falip M. *et al.* Expert opinion on the Management of Lennox–Gastaut Syndrome: treatment algorithms and practical considerations. *Front Neurol* 2017;**8**.

14. Kovacevic J, Maroteaux G, Schut D. *et al.* Protein instability, haploinsufficiency, and cortical hyper-excitability underlie STXBP1 encephalopathy. *Brain* 2018;**141**:1350–74.

15. Chambers SM, Fasano CA, Papapetrou EP. *et al.* Highly efficient neural conversion of human ES and iPS cells by dual inhibition of SMAD signaling. *Nat Biotechnol* 2009;**27**:275–80.

16. Hulme AJ, Maksour S, St-Clair Glover M. *et al.* Making neurons, made easy: the use of Neurogenin-2 in neuronal differentiation. *Stem Cell Reports* 2022;**17**:14–34.

17. Meijer M, Rehbach K, Brunner JW. *et al.* A single-cell model for synaptic transmission and plasticity in human iPSC-derived neurons. *Cell Rep* 2019;**27**:2199–2211.e6.

18. Nehme R, Zuccaro E, Ghosh SD. *et al.* Combining NGN2 programming with developmental patterning generates human excitatory neurons with NMDAR-mediated synaptic transmission. *Cell Rep* 2018;**23**:2509–23.

19. Thoma EC, Wischmeyer E, Offen N. *et al.* Ectopic expression of neurogenin 2 alone is sufficient to induce differentiation of embryonic stem cells into mature neurons. *PLoS One* 2012; **7**:e38651.

20. Zhang Y, Pak C, Han Y. *et al.* Rapid single-step induction of functional neurons from human pluripotent stem cells. *Neuron* 2013;**78**:785–98.

21. Weisheit I, Kroeger JA, Malik R. *et al.* Detection of deleterious on-target effects after HDR-mediated CRISPR editing. *Cell Rep* 2020;**31**:107689.

22. Weisheit I, Kroeger JA, Malik R. *et al.* Simple and reliable detection of CRISPR-induced on-target effects by qgPCR and SNP genotyping. *Nat Protoc* 2021;**16**:1714–39.

23. Bekkers JM, Stevens CF. Excitatory and inhibitory autaptic currents in isolated hippocampal neurons maintained in cell culture. *Proc Natl Acad Sci USA* 1991;**88**:7834–8.

24. Dobrunz LE, Stevens CF. Heterogeneity of release probability, facilitation, and depletion at central synapses. *Neuron* 1997;**18**: 995–1008.

25. Zucker RS, Regehr WG. Short-term synaptic plasticity. *Annu Rev Physiol* 2002;**64**:355–405.

26. Dittman JS, Kreitzer AC, Regehr WG. Interplay between facilitation, depression, and residual calcium at three presynaptic terminals. *J Neurosci* 2000;**20**:1374–85.

27. Berkel AAV, Lammertse HCA, Öttl M. *et al.* Reduced MUNC18-1 levels, synaptic proteome changes and altered network activity

in STXBP1-related disorder patient neurons. *Biol Psychiatry Glob Open Sci* 2023;**4**:284–98.

28. Saitsu H, Kato M, Okada I. *et al.* STXBP1 mutations in early infantile epileptic encephalopathy with suppression-burst pattern. *Epilepsia* 2010;**51**:2397–405.

29. Martin S, Papadopulos A, Tomatis VM. *et al.* Increased Polyubiquitination and proteasomal degradation of a Munc18-1 disease-linked mutant causes temperature-sensitive defect in exocytosis. *Cell Rep* 2014;**9**:206–18.

30. Guiberson NGL, Pineda A, Abramov D. *et al.* Mechanism-based rescue of Munc18-1 dysfunction in varied encephalopathies by chemical chaperones. *Nat Commun* 2018;**9**:3986.

31. André T, Classen J, Brenner P. *et al.* The interaction of Munc18-1 helix 11 and 12 with the central region of the VAMP2 SNARE motif is essential for SNARE templating and synaptic transmission. *eNeuro* 2020;**7**:ENEURO.0278–20.2020.

32. Gong J, Wang X, Cui C. *et al.* Exploring the two coupled conformational changes that activate the Munc18-1/Syntaxin-1 complex. *Front Mol Neurosci* 2021;**14**:785696.

33. Han GA, Bin N-R, Kang S-YA. *et al.* Domain 3a of Munc18-1 plays a crucial role at the priming stage of exocytosis. *J Cell Sci* 2013;**126**:2361–71.

34. Han GA, Park S, Bin N-R. *et al.* A pivotal role for pro-335 in balancing the dual functions of Munc18-1 domain-3a in regulated exocytosis. *J Biol Chem* 2014;**289**:33617–28.

35. Hu S-H, Christie MP, Saez NJ. *et al.* Possible roles for Munc18-1 domain 3a and Syntaxin1 N-peptide and C-terminal anchor in SNARE complex formation. *Proc Natl Acad Sci USA* 2011;**108**:1040–5.

36. Martin S, Tomatis VM, Papadopulos A. *et al.* The Munc18-1 domain 3a loop is essential for neuroexocytosis but not for syntaxin-1A transport to the plasma membrane. *J Cell Sci* 2013;**126**:2353–60.

37. Munch AS, Kedar GH, van Weering JRT. *et al.* Extension of helix 12 in Munc18-1 induces vesicle priming. *J Neurosci* 2016;**36**:6881–91.

38. Parisotto D, Pfau M, Scheutzow A. *et al.* An extended helical conformation in domain 3a of Munc18-1 provides a template for SNARE (soluble N-ethylmaleimide-sensitive factor attachment protein receptor) complex assembly. *J Biol Chem* 2014;**289**:9639–50.

39. Wang X, Gong J, Zhu L. *et al.* Identification of residues critical for the extension of Munc18-1 domain 3a. *BMC Biol* 2023;**21**:158.

40. Meijer M, Dörr B, Lammertse HC. *et al.* Tyrosine phosphorylation of Munc18-1 inhibits synaptic transmission by preventing SNARE assembly. *EMBO J* 2018;**37**:300–20.

41. Graham ME, Prescott GR, Johnson JR. *et al.* Structure-function study of mammalian Munc18-1 and C. elegans UNC-18 implicates domain 3b in the regulation of exocytosis. *PLoS One* 2011;**6**:e17999.

42. Li W, Xing Y, Wang Y. *et al.* A non-canonical target-binding site in Munc18-1 domain 3b for assembling the Mint1-Munc18-1-syntaxin-1 complex. *Structure* 2023;**31**:68–77.e5.

43. Weeratunga S, Gormal RS, Liu M. *et al.* Interrogation and validation of the interactome of neuronal Munc18-interacting mint proteins with AlphaFold2. *J Biol Chem* 2023;**300**:105541.

44. Graham ME, Handley MTW, Barclay JW. *et al.* A gain-of-function mutant of Munc18-1 stimulates secretory granule recruitment and exocytosis and reveals a direct interaction of Munc18-1 with Rab3. *Biochem J* 2008;**409**:407–16.

45. Dukkipati SS, Garrett TL, Elbasiouny SM. The vulnerability of spinal motoneurons and soma size plasticity in a mouse model of amyotrophic lateral sclerosis. *J Physiol* 2018;**596**:1723–45.

46. Rhee HJ, Shaib AH, Rehbach K. *et al.* An Autaptic culture system for standardized analyses of iPSC-derived human neurons. *Cell Rep* 2019;**27**:2212–2228.e7.

47. Oswald A-MM, Reyes AD. Maturation of intrinsic and synaptic properties of layer 2/3 pyramidal neurons in mouse auditory cortex. *J Neurophysiol* 2008;**99**:2998–3008.

48. Sabogal-Guáqueta AM, Marmolejo-Garza A, Trombetta-Lima M. *et al.* Species-specific metabolic reprogramming in human and mouse microglia during inflammatory pathway induction. *Nat Commun* 2023;**14**:6454.

49. Brunner JW, Lammertse HCA, van Berkel AA. *et al.* Power and optimal study design in iPSC-based brain disease modelling. *Mol Psychiatry* 2023;**28**:1545–56.

50. Fu S, Bury LAD, Eum J. *et al.* Autism-specific PTEN p.Ile135Leu variant and an autism genetic background combine to dysregulate cortical neurogenesis. *Am J Hum Genet* 2023;**110**:826–45.

51. Carcamo-Orive I, Hoffman GE, Cundiff P. *et al.* Analysis of transcriptional variability in a large human iPSC library reveals genetic and non-genetic determinants of heterogeneity. *Cell Stem Cell* 2017;**20**:518–532.e9.

52. DeBoever C, Li H, Jakubosky D. *et al.* Large-scale profiling reveals the influence of genetic variation on gene expression in human induced pluripotent stem cells. *Cell Stem Cell* 2017;**20**:533–546.e7.

53. Kilpinen H, Goncalves A, Leha A. *et al.* Common genetic variation drives molecular heterogeneity in human iPSCs. *Nature* 2017;**546**:370–5.

54. Brinkman EK, Chen T, Amendola M. *et al.* Easy quantitative assessment of genome editing by sequence trace decomposition. *Nucleic Acids Res* 2014;**42**:e168.

55. Marshall CR, Howrigan DP, Merico D. *et al.* Contribution of copy number variants to schizophrenia from a genome-wide study of 41,321 subjects. *Nat Genet* 2017;**49**:27–35.

56. Schmid B, Holst B, Poulsen U. *et al.* Generation of two gene edited iPSC-lines carrying a DOX-inducible NGN2 expression cassette with and without GFP in the AAVS1 locus. *Stem Cell Res* 2021;**52**:102240.